ARCTIC CLIMATE

Fluctuating Atlantic inflows modulate Arctic atlantification

Igor V. Polyakov[1]*, Randi B. Ingvaldsen[2], Andrey V. Pnyushkov[3], Uma S. Bhatt[4], Jennifer A. Francis[5], Markus Janout[6], Ronald Kwok[7], Øystein Skagseth[2,8]

Enhanced warm, salty subarctic inflows drive high-latitude atlantification, which weakens oceanic stratification, amplifies heat fluxes, and reduces sea ice. In this work, we show that the atmospheric Arctic Dipole (AD) associated with anticyclonic winds over North America and cyclonic winds over Eurasia modulates inflows from the North Atlantic across the Nordic Seas. The alternating AD phases create a "switchgear mechanism." From 2007 to 2021, this switchgear mechanism weakened northward inflows and enhanced sea-ice export across Fram Strait and increased inflows throughout the Barents Sea. By favoring stronger Arctic Ocean circulation, transferring freshwater into the Amerasian Basin, boosting stratification, and lowering oceanic heat fluxes there after 2007, AD+ contributed to slowing sea-ice loss. A transition to an AD– phase may accelerate the Arctic sea-ice decline, which would further change the Arctic climate system.

The Arctic region is rightfully called a frontier for global climate change. Linked to atmospheric circulation, radiative forcing, and a host of climate feedback mechanisms, Arctic surface air temperatures are rising at least three times faster than global-average air temperatures (*1*). The Arctic Ocean is warming faster than the global ocean (*2*). Sea-ice decline is a true indicator of climate change, affecting all aspects of life in the northern high-latitude regions (*1*). One of the reasons for sea-ice loss is the warming Arctic Ocean, which is caused in part by anomalous inflows from the North Atlantic and North Pacific (*3*–*5*). System-wide changes in Arctic basins caused by anomalous inflows from the Nordic Seas are referred to as atlantification (*5*–*7*). One of the many manifestations of atlantification in the Eurasian Basin of the Arctic Ocean is decreased upper-ocean stratification and enhanced heat release from the warm intermediate (150- to 800-m depth) Atlantic water layer, which results in accelerated loss of sea ice (*5*, *8*, *9*). However, these changes are complex, and their driving forces and interactions with the Arctic atmosphere–ice–ocean system are not well understood. This study identifies important mechanisms that steer high-latitude atlantification, which inform a broad and comprehensive understanding of system function.

[1]International Arctic Research Center and College of Natural Science and Mathematics, University of Alaska Fairbanks, Fairbanks, AK 99775, USA. [2]Institute of Marine Research, Bergen, Norway. [3]International Arctic Research Center, University of Alaska Fairbanks, Fairbanks, AK 99775, USA. [4]Geophysical Institute and College of Natural Science and Mathematics, University of Alaska Fairbanks, Fairbanks, AK 99775, USA. [5]Woodwell Climate Research Center, Falmouth, MA 02540, USA. [6]Alfred-Wegener-Institute, Helmholtz Centre for Polar and Marine Research, D-27570 Bremerhaven, Germany. [7]Polar Science Center, Applied Physics Laboratory, University of Washington, Seattle, WA 98105, USA. [8]Bjerknes Centre for Climate Research, Bergen, Norway.
*Corresponding author. Email: ivpolyakov@alaska.edu

Sea-ice changes

Although the end-of-summer ice extent and thickness are declining, our results indicate that the rate of decline slowed after 2007 compared with 1992 to 2006 (Fig. 1, A and B). Over the satellite record, the trend in summer ice extent during 2007 to 2021 ($-0.07 \pm 0.18 \times 10^6$ km^2 per decade) is weak and not statistically significant in contrast to the much larger negative trends in 1979 to 2021 ($-0.79 \pm 0.13 \times 10^6$ km^2 per decade) and 1992 to 2006 ($-0.99 \pm 0.51 \times 10^6$ km^2 per decade). Thus, a more stable regime of Arctic sea ice appears to have begun in 2007. This transition was abrupt, with 2007 setting a record for a single-year sea-ice–extent decrease of -1.6×10^6 km^2 (compare with 2012's second record-year drop of -1.0×10^6 km^2) (*10*).

Similarly, the composite record of mean winter (February to March) ice thickness in the central Arctic, now close to ~2 m, has not changed markedly since 2007 (Fig. 1A), even though the multidecadal decline has been significant. In addition, the mean thickness in fall (October to November) has remained above the 1-m low established after the end of the summer of 2007. Between 2003 and 2007, the thinning was notable and occurred with the loss of a large fraction of thick multiyear sea ice (*11*). The overall thinning has slowed since 2007, when satellite-based records of ice thickness began (ICESat, ICESat-2, and CryoSat-2, 2003 to 2021). The Arctic is now dominated by the behavior of thinner seasonal ice, which now solely controls the variability of ice thickness in the central Arctic (*12*, *13*).

Atmospheric changes

The atmosphere over the Arctic Ocean is dominated by high pressure (known as the Polar High) centered over the western Arctic (Fig. 2A), which generates a mean anticyclonic (clockwise) circulation. This drives predominant features of sea-ice drift and upper-ocean circulation known as the Beaufort Gyre in the Amerasian Basin as well as the Transpolar Drift flowing from the Siberian shelf toward the Canadian Archipelago and Fram Strait (Fig. 1G).

The primary mode of variability of the pan-Arctic sea level pressure is known as the Arctic Oscillation, and the related wind pattern accounts for the observed climatological features of the atmospheric circulation. Beginning in 2007, however, the secondary Arctic Dipole (AD) pattern, which features higher sea level pressure over the Beaufort Gyre and the Canadian Archipelago along with lower sea level pressure over the Siberian Arctic, became dominant [Fig. 2C; see also (*14*–*16*)], whereas the Arctic Oscillation remained close to neutral (fig. S4). This shift is evident in the higher spatial correlation between the mean 2007 to 2021 sea level pressure and the AD ($R = 0.59$, where R is the correlation coefficient), compared to that with the Arctic Oscillation ($R = 0.47$).

The AD index, a characteristic of the wind cyclonicity in the central and Siberian Arctic (*14*), varies between positive (AD+) and negative (AD–) over ~15-year regimes (see wavelets in figs. S2 and S3). During 1992 to 2006, both the AD and Arctic Oscillation spring-summer indices were slightly negative (fig. S4, D and E), whereas during 2007 to 2021, the AD index became increasingly positive (fig. S4E).

The AD+ drives an enhanced anticyclonic Beaufort Gyre and Transpolar Drift (Fig. 2) (*17*). Distinct from the Arctic Oscillation (*18*, *19*), the across-pole AD pattern results in increased heat advection into the Arctic, especially along the Siberian shores (Fig. 2B), and contributes to higher surface air temperatures (fig. S3). The AD was a major driver of the second record-low sea-ice extent in summer 2007 during the satellite record (*20*). The Fram Strait sea-ice export is correlated with the AD index during 1979 to 2014 [significant $R = 0.45$, (*17*); see Fig. 2D], with a stronger link to the AD than to the Arctic Oscillation (*21*).

Most important for this study, the alternating AD phases were pivotal for a switchgear mechanism that modulates the relative strength of the Fram Strait and Barents Sea branches transporting Atlantic water into the Arctic Ocean. For example, the anomalous atmospheric forcing during the AD+ in 2007 to 2021 was favorable for reduced flows into the Arctic through the Fram Strait along with enhanced inflows through the Barents Sea Opening (Fig. 2, B, E, and F). The Arctic Oscillation pattern contributes to large-scale cyclonicity in Arctic atmosphere, ocean, and ice circulation (*22*) but not the finer details suggested by the switchgear mechanism discussed here (fig. S4). The AD-driven forcing is best developed in spring and summer (figs. S2 and S5) but can affect air temperatures,

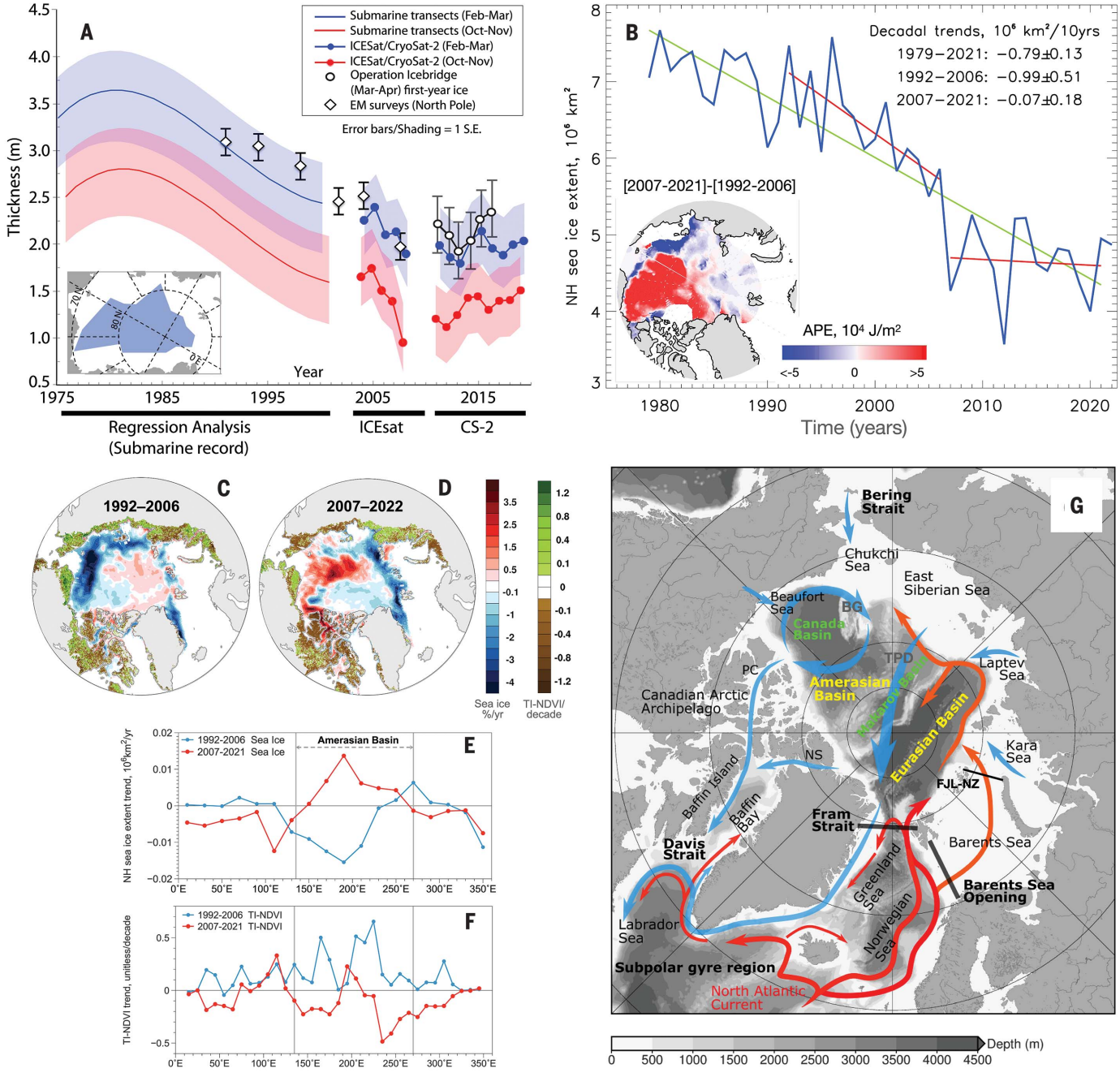

Fig. 1. Loss of Arctic sea-ice thickness and extent. (**A**) Arctic sea ice thickness changes for autumn (red and dotted red) and winter (blue and dotted blue). Shadings (blue and red) show 1 standard error (S.E.) ranges from the regression analysis of submarine ice thickness and expected uncertainties in satellite ice thickness estimates. Data release area of submarine data ice thickness data are shown in the inset. Satellite ice thickness estimates are for the Arctic south of 88°N. Thickness estimates from more localized airborne/ground electromagnetic surveys near the North Pole (diamonds) and from Operation IceBridge (circles) are shown within the context of the larger scale changes in the submarine and satellite records (*52*). EM, electromagnetic. (**B**) September Northern Hemisphere (NH) sea-ice extent (blue line), the long-term trend (green line), and different regimes of sea-ice extent change in 1992 to 2006 and 2007 to 2021 (red segments); the inset shows available potential energy (APE) anomalies in the upper ocean (surface mixed layer and halocline) for 2007 to 2017 relative to 1992 to 2006 (increasing APE signifies stronger stratification suppressing mixing). (**C** and **D**) Maps of trends for the sea-ice concentration (percentage per year) and the summer biweekly (time-integrated) TI-NDVI (decade^{-1}) over Arctic tundra for 1992 to 2006 (C) and 2007 to 2021 (D). The NDVI is a proxy for vegetation productivity and is derived from remotely sensed products. A positive NDVI trend means that the vegetation has more biomass and more photosynthetic productivity; this process is called greening. A negative NDVI trend means that the vegetation has less biomass and is less healthy, and it is called browning. (**E** and **F**) September sea-ice extent trends (E) and the TI-NDVI (F) for 1992 to 2006 (blue) and 2007 to 2021 (red) as a function of longitude. (**G**) Diagram of sea ice drift and upper ocean circulation (blue arrows), as well as Atlantic water circulation (red arrows) (*53*). FJL-NZ, TPD, and BG indicate Franz Joseph Land–Novaya Zemlya pass, TransPolar Drift, and Beaufort Gyre, respectively.

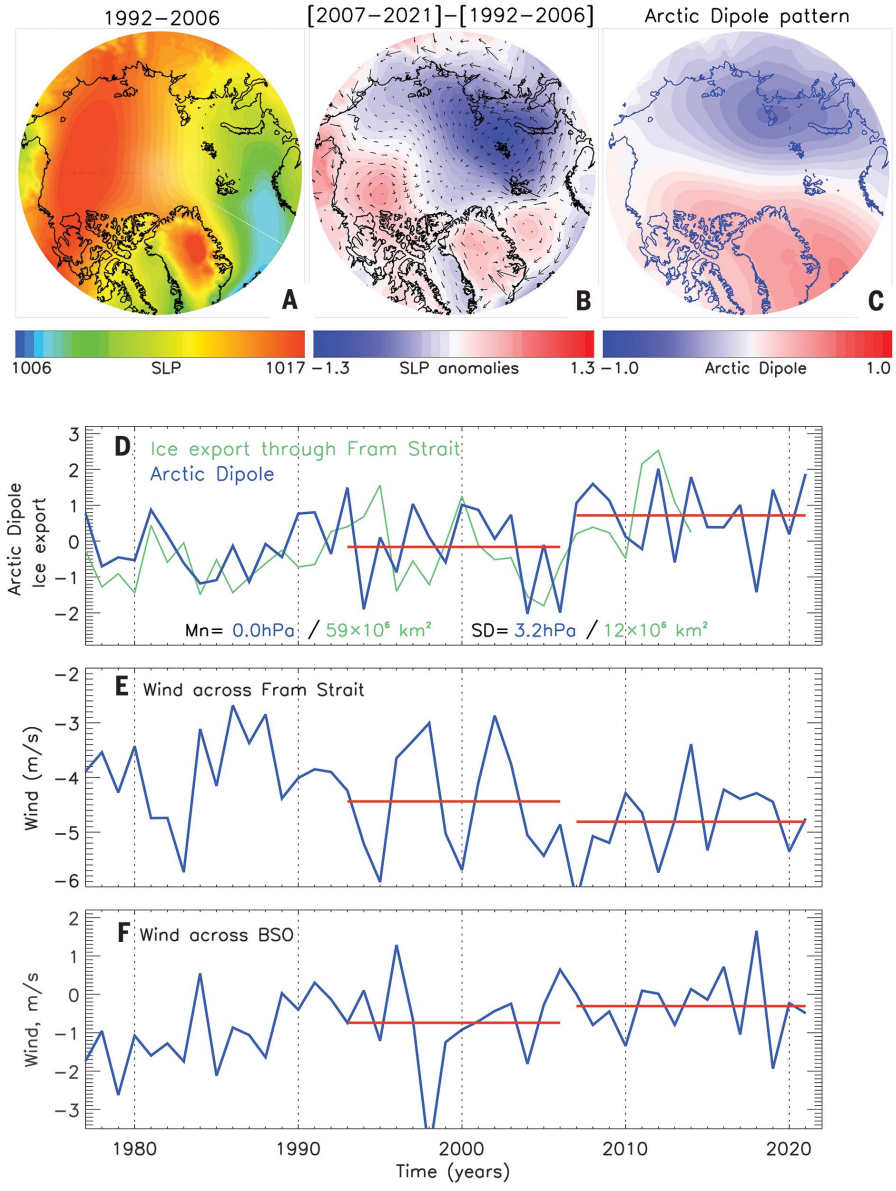

Fig. 2. Atmospheric forcing governing the switchgear mechanism. (**A**) Annual sea level pressure (SLP)(hPa) averaged over 1992 to 2006. (**B**) Annual pressure anomalies (hPa, shading) in 2007 to 2021 relative to 1992 to 2006. Vectors show corresponding anomalous geostrophic winds. (**C**) April to July AD (hPa) pattern, which is correlated with the 2007 to 2021 pressure anomalies at R = 0.59. (**D** to **F**) Time series of atmospheric parameters. (D) April to July AD (blue) and March to August ice area transport across Fram Strait [green, from (*19*)] are reduced to anomalies by subtracting means (Mn) and normalized by SDs; AD and ice export are correlated at R = 0.44. (E and F) Annual wind across Fram Strait (E) and Barents Sea Opening (BSO) (F). In (D) to (F), red horizontal segments show 1992 to 2006 and 2007 to 2021 means.

surface energy fluxes, storm tracks, sea-ice drift and exports, and upper-ocean circulation in all seasons (fig. S3).

Changes in the Arctic Ocean

Switchgear mechanism between the Fram Strait inflow and Barents Sea throughflow

Water exchanges between the Nordic Seas and the Arctic Ocean are critically important for the state of the Arctic climate system. Ocean Reanalysis System 5 (ORAS5) reanalysis data (see the supplementary materials for details) suggest that these exchanges in the upper 50 m were amplified across the northern Barents Sea Opening and in the northern and central Barents Sea while being reduced across the Fram Strait in the past 15 years (Fig. 3), with similar patterns but weaker anomalies in the 50- to 200-m layer (fig. S6). A time series of currents across the Barents Sea Opening and Fram Strait clearly show this alternating pattern, with 5% increased annual mean currents in the Barents Sea Opening and 15% decrease in the Fram Strait (Fig. 3, C and D). Summer and fall ORAS5 transports were the most notable contributors to anomalous Barents Sea Opening inflows (15% increase), whereas spring and summer processes dominated Atlantic water inflows through the Fram Strait (28% decrease in current speed) (fig. S7). At the 95% confidence level, each of the aforementioned estimates of anomalous transports is statistically significant. In comparison to the Barents Sea Opening, changes in the upper 50-m water volume transports were ~2.2 times as strong in the Fram Strait. As a result, changes in transports through these gateways do not countervail, and the importance of other gateways in establishing the Arctic Ocean's water balance must not be underestimated. On weekly to monthly timescales, increased eastward flow in the northern Barents Sea and weakened inflow across the Fram Strait are associated with a northward shift in atmospheric cyclones over the Barents Sea (*23*).

Amplified Barents Sea Opening inflows in 2007 to 2021 resulted in increased transports across the Franz Joseph Land–Novaya Zemlya pass by 23%, thus providing an enhanced inflow from the Barents Sea into the Arctic Ocean (Fig. 3G and fig. S8). These changes were crucial for the new state of the eastern Arctic Ocean brought on by atlantification (*5*). Tracer experiments showed a doubled probability that water parcels in the upper 50 m crossed the Barents Sea in 2007 to 2021 compared with 1992 to 2006, in contrast with the Fram Strait, where the number of tracers decreased over the same time by a factor of four (Fig. 4, D and E). Stronger impacts of the local winds on the Barents Sea compared with Fram Strait inflows are consistent with stronger topographic steering and more complex flow in the Fram Strait (*24*, *25*).

These findings are strongly supported by both in situ and satellite observations. For example, mooring and reanalysis records are positively correlated and show consistent increasing (decreasing) trends of currents across the Barents Sea Opening (Fram Strait) over the past 15 years (fig. S9). A modest correlation R = 0.34 between the Barents Sea Opening mooring and reanalysis time series is likely because moorings do not cover the northern regions where the reanalysis shows the greatest increase in flow. Moreover, anomalies in the satellite-based sea surface height provide further confirmation for the switchgear mechanism modulating the inflows through the Barents Sea and Fram Strait during the current AD+ (Fig. 4G). Geostrophic currents forced by the anomalous 2007 to 2021 sea surface height were amplified in the northern Barents Sea Opening and in the central Barents Sea but showed little

difference in the southern Barents Sea Opening. However, the sea surface height indicates an anomalous flow from the Lofoten Basin to the Barents Sea in 2007 to 2020 (Fig. 4G). The possibility of the Lofoten Basin feeding the Barents Sea has been suggested by (*26*), attributed to the vigorous eddy activity in the Lofoten Basin (*27*, *28*), and is further linked to the atmospheric wind forcing (*29*). In contrast to the Barents Sea Opening, the geostrophic flow across the Fram Strait weakened (Fig. 4G).

Imprints of alternating AD patterns on the Arctic Ocean circulation

The Arctic basins responded to the AD+ atmospheric regime in 2007 to 2021 with basin-wide changes in the upper Arctic Ocean circulation associated with an amplified Beaufort Gyre, stronger boundary currents along the Siberian slope, and a shifted Transpolar Drift from the Amerasian Basin toward the Lomonosov Ridge (Fig. 3B and Fig. 4, A and B).

Since 2007, a smaller but more intense Arctic high, associated wind-driven circulation, and convergence of the upper Beaufort Gyre have resulted in enhanced freshening and thickening of the surface fresh layer in the Amerasian Basin (*22*, *30*). The Beaufort Gyre mooring record provides confirmation of these findings (Fig. 5, A and B). This evidence is further supported by observed sea-ice melt, redirected Siberian riverine waters into the Beaufort Gyre, increasing inflow of relatively fresh Pacific Water through the Bering Strait, and strengthened stratification between the Amerasian Basin's surface and deep layers (*22*, *30*–*32*). At the same time, reanalysis and mooring observations showed contrasting changes in the Eurasian Basin, with increased salinification and weakened stratification in the halocline, along with amplified upward heat fluxes (Fig. 5, C and D) (*5*, *33*).

Our tracer experiments support these findings (Fig. 4, A to C, and fig. S11). For example, the 2007 to 2021 cyclonic atmospheric forcing widely dispersed transports of freshwater from the Siberian shelves (where the Transpolar Drift originates) and drove a substantial portion (17% of all trajectories) of the Siberian freshwater into the Beaufort Gyre. By contrast, during the anticyclonic 1992 to 2006 AD– phase, not a single water parcel ended up trapped in the Beaufort Gyre, and they instead left the central Arctic through the straits of the Canadian Archipelago. Changes in the spatial distributions of meteoric water (i.e., precipitation including water from lakes and rivers) provide confirmation of the diversion of freshwater from the Eurasian Basin to the Amerasian Basin, with meteoric water content decreasing in the Eurasian Basin and increasing in the Amerasian Basin, consistent with (*34*, *35*). These changes in meteoric water content are accompanied by a general increase in net sea-ice meltwater (fig. S12).

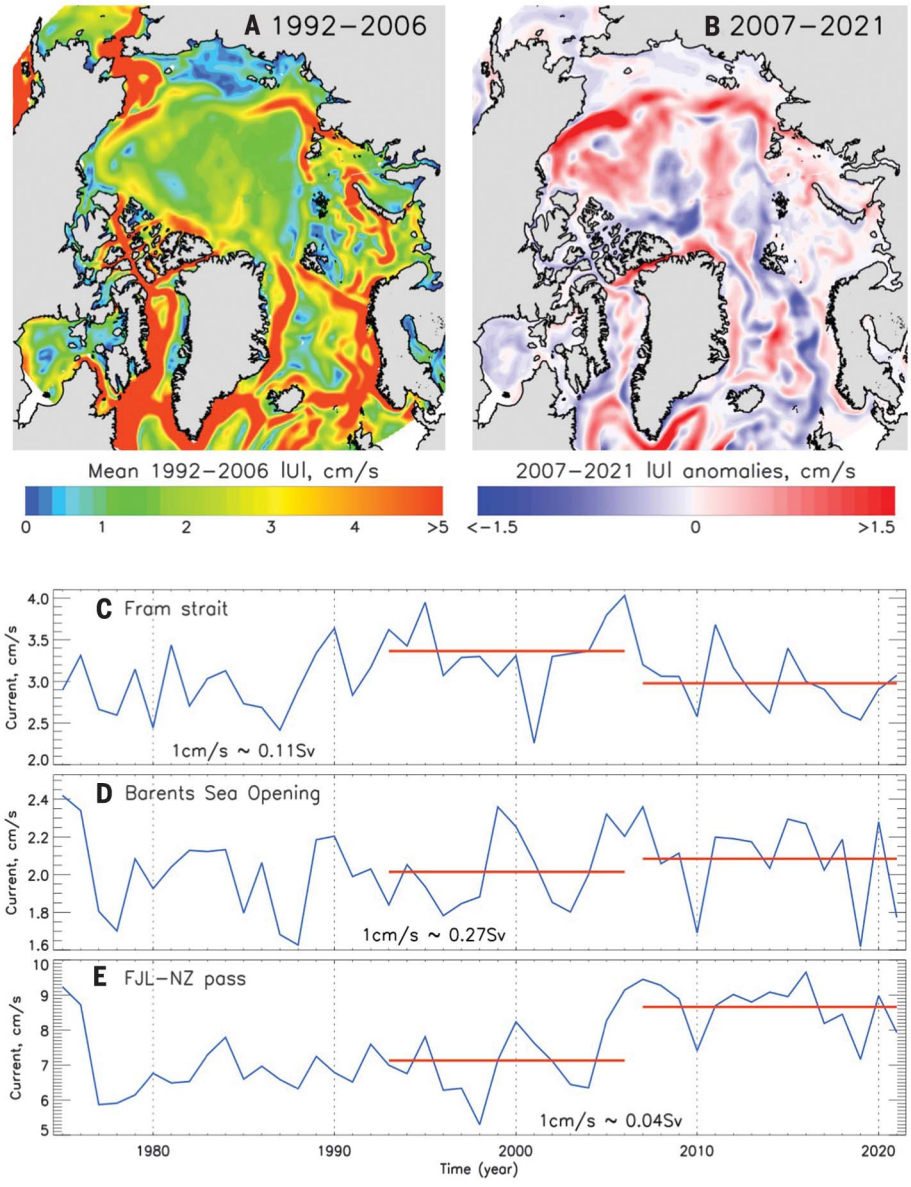

Fig. 3. Changes in upper 50 m oceanic circulation from ORAS5 reanalysis between alternate AD phases. (**A** and **B**) Maps of (A) 1992 to 2006 annual mean current speed |U| and (B) 2007 to 2021 |U| anomalies (relative to the 1992 to 2006 mean) of the Arctic Ocean and Nordic Seas region with removed low-frequency (1/30 years cut-off frequency) components by using running mean filtering. (**C** to **E**) Time series of the ocean annual mean currents inflowing into the Arctic through Fram Strait (80°N, 14°W to 10°E) (C), the Barents Sea Opening (71°N to 77°N, 20°E) (D), and the FJL–NZ passage (76.7°N to 80.6°N, 60.5°E to 64.3°E) (E). Red horizontal lines show means over 1992 to 2006 and 2007 to 2021. Transfer coefficients from current in centimeters per second to water transport in sverdrups (Sv) (1 Sv = 10^6 m^3/s) are given in each time series panel. Note the reduced (enhanced) inflow through Fram Strait and enhanced (reduced) Barents Sea throughflow in the years 2007 to 2021 (1992 to 2006).

In the Eurasian Basin, the local effects of alternating AD patterns and the remote effects of atlantification owing to changing influxes across Fram Strait and Barents Sea are interconnected in an ice/ocean heat feedback mechanism. Weakened stratification and increased oceanic heat fluxes associated with atlantification drive sea-ice melt, which is amplified by increased oceanic heat fluxes through increased convective entrainment in winter (*5*, *9*). A stronger coupling between atmosphere, ice, and ocean in the eastern Arctic in the recent decade and intensified upper-ocean currents play critical roles in developing this feedback (Fig. 3B) (*36*).

Changes in the Nordic Seas

Anomalous anticyclonic winds over the Nordic Seas, as evident during the AD+ in 2007 to 2021

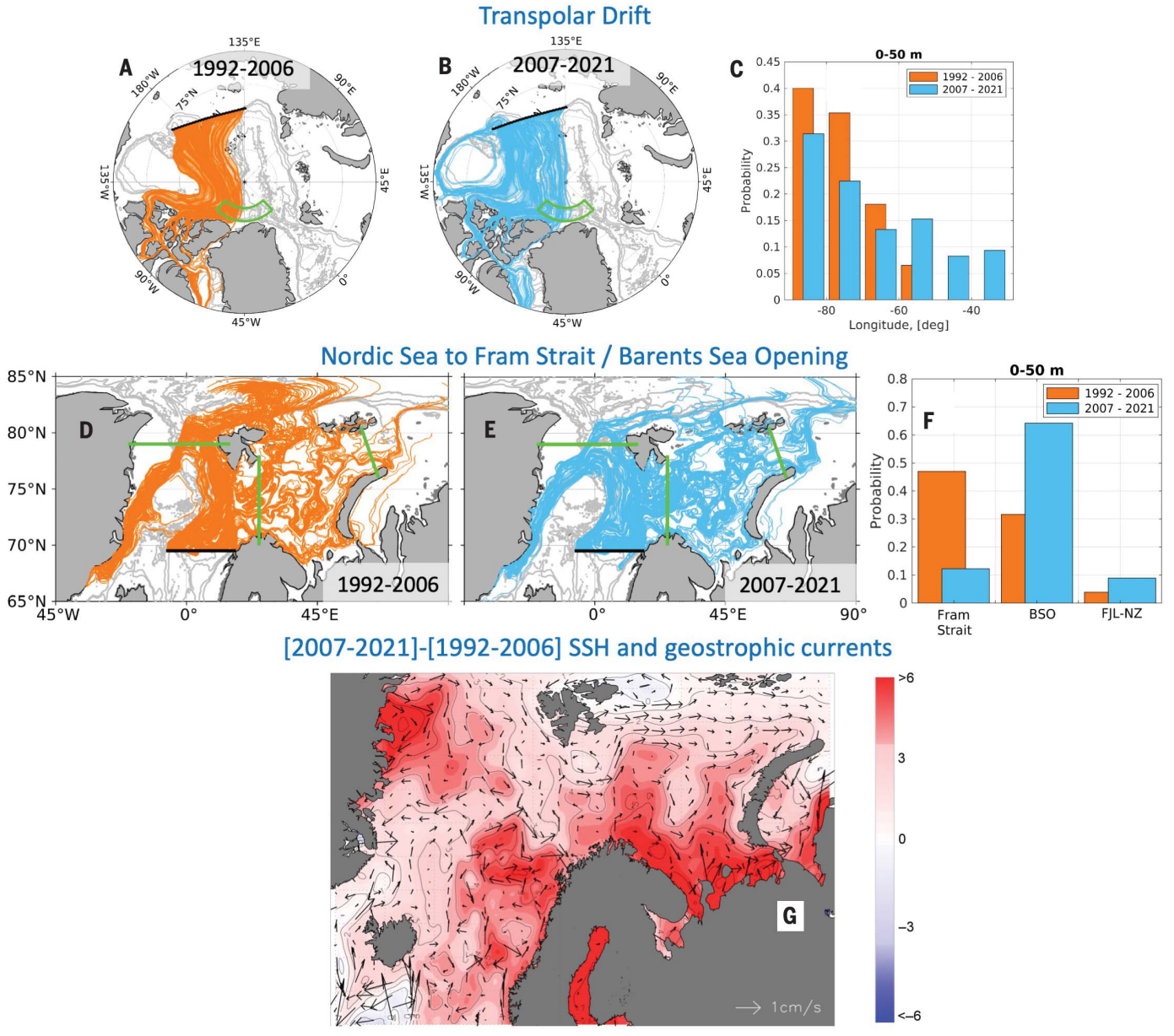

Fig. 4. Difference of the oceanic circulation patterns between alternate AD phases. (**A** to **G**) A shift in the Transpolar Drift [(A) to (C)], inflows of Atlantic water from the Nordic Seas across the Barents Sea Opening and Fram Strait [(D) to (F)], and anomalous (2007 to 2021 minus 1992 to 2006) sea surface height (SSH) (cm) and corresponding geostrophic currents (G). (A to C) ORAS5-based trajectories of parcels exiting the central Siberian shelf in 1992 to 2006 (A) and 2007 to 2021 (B) and the probability of finding a parcel within the polygon (indicated with the green line) north of the Canadian Archipelago (C). (D to F) ORAS5-based trajectories of parcels released in the Nordic Seas along the sections indicated with the black line in 1992 to 2006 (D) and 2007 to 2021 (E) and the probability of finding a parcel traveling across the Barents Sea Opening, Fram Strait, and FJL–NZ [indicated with the green lines in (D) and (E)]. (G) Satellite-based anomalous SSH and geostrophic currents showing the switchgear mechanism from Fram Strait to Barents Sea Opening inflow after 2007.

(Fig. 2B), weakened the poleward Atlantic water flow from south of the subpolar gyre and through the Nordic Seas (*25*, *37*). Attributed to a weak reinforcement of the subpolar gyre (fig. S13) that altered the properties of the inflowing Atlantic water (*38*), the Atlantic water inflow from the northern North Atlantic became colder and fresher in the late 2000s (Fig. 5, Q and R) (*39*). The Atlantic water temperatures and salinities in the Nordic Seas and the Barents Sea Opening responded to this change by peaking in the late 2000s (Fig. 5, K to P).

Consistent with these changes, the salinity trends in the Nordic Seas after 2006/2007 are negative and similar in magnitude from the North Atlantic up to the Barents Sea Opening (Fig. 5, R, P, N, J, and I). Atmospheric circulation over the Nordic Seas associated with the AD+ in 2007 to 2021 (Fig. 2B) weakened the northward Norwegian Atlantic Current (Fig. 3B) (*40*), which is consistent with a negative trend of –3 cm/s per decade shown by the mooring record from the Svinøy section, the gateway for the Atlantic water into the Nordic Seas (fig. S9). Despite these changes in the Nordic Seas, the salinity in the eastern Eurasian Basin halocline and Atlantic water increased (Fig. 5D), driven by salinification in the upstream northern Barents Sea due to lack of meltwater input from seasonal ice melt (*41*).

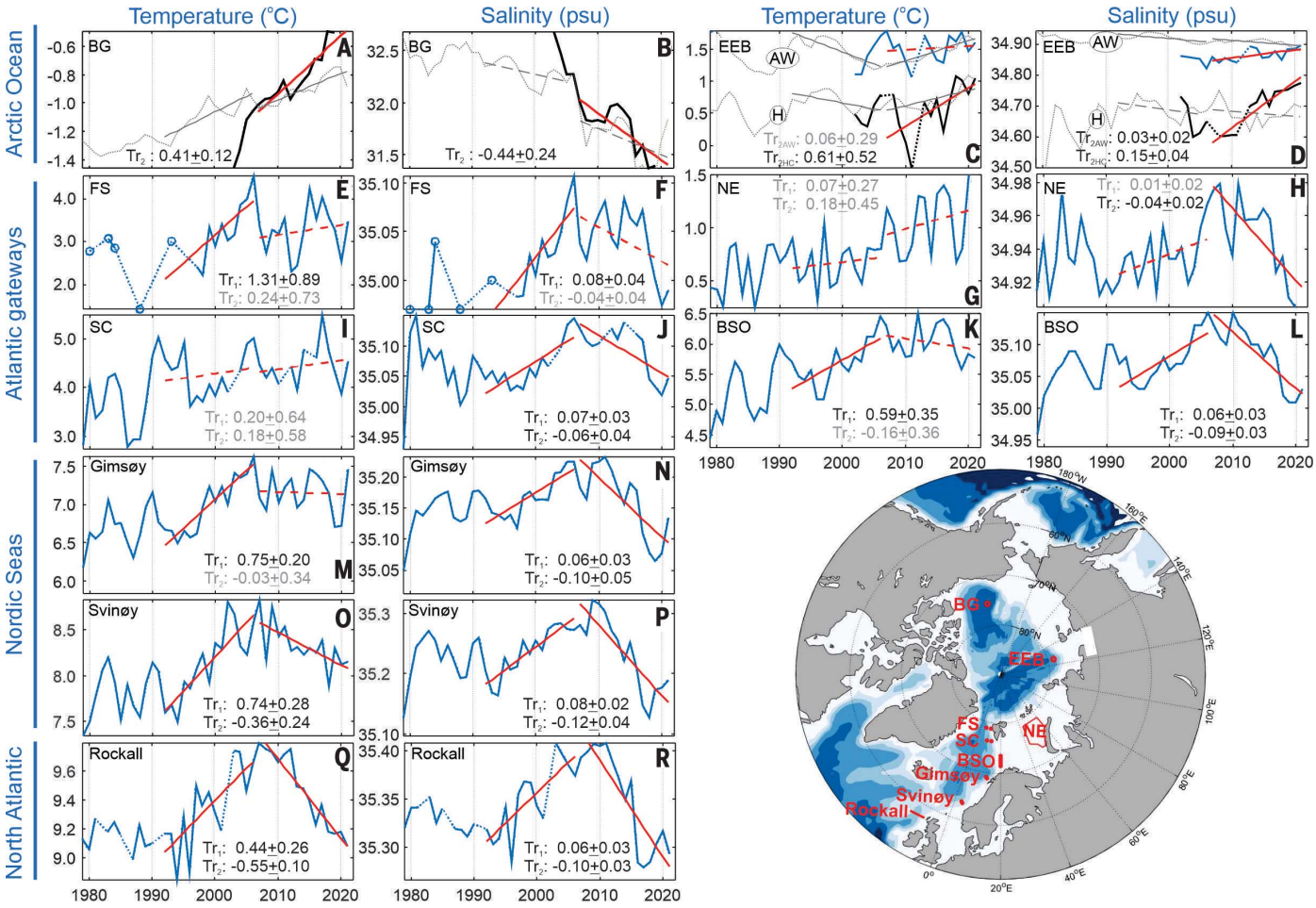

Fig. 5. Contrasting trends of ocean temperature and salinity in the region spanning from the northern North Atlantic to the Arctic Ocean during the positive (2007 to 2021) and negative (1992 to 2006) phases of the AD. (**A** to **R**) Annual time series of water temperature and salinity from repeated observations from the Atlantic water layer (for depth ranges, see supplementary materials; blue lines) and halocline (150 m, black lines) (see details in materials and methods). Observations with substantial gaps were complemented by ORAS5 reanalysis time series [gray lines; for the eastern Eurasian Basin (EEB), we plotted ORAS5 temperature, adding 1°C]. Ninety-five percent statistically significant trends are shown by solid red lines and black font; otherwise, dashed red lines and gray font are used. The Beaufort Gyre (BG), Barents Sea Opening (BSO), Fram Strait (FS), South Cape (SC), and North Eastern (NE) Barents Sea are indicated on the map.

The cooling trend in 2007 to 2021 is reduced along stream the Atlantic water from the northern North Atlantic into the Barents Sea and Fram Strait (−0.55°C in the North Atlantic/Rockall, −0.36°C at Svinøy, and insignificant farther north; Fig. 5). These changes in the Nordic Seas are supported by the reduced oceanic heat loss over the past decades (*42*). Thus, the traditional paradigm of Atlantic water variability associated with either cold and fresh or warm and saline Atlantic water has changed (Fig. 5, E to N). Moreover, our analysis confirms a northward amplification of oceanic warming (*7*), with the origin in the Nordic Seas, which makes this a source region of atlantification and Arctic amplification.

The observed temperature and salinity trends are also consistent with the switchgear-driven stronger flow through the Barents Sea Opening compared with Fram Strait flow after 2006/2007, with temperatures at the Barents Sea Opening and northeastern Barents Sea showing little or no decrease (Fig. 5, G and K), whereas the Fram Strait temperatures fell rapidly (Fig. 5, E and I). Since the mid-2000s, the along-track heat loss of the Fram Strait inflow has increased (*43*), whereas the heat loss of the Barents Sea throughflow has decreased or remained stable (*43*, *44*), which thereby implies a stronger warming of the Atlantic water entering the Arctic from the Barents Sea as compared with Fram Strait. Thus, a combination of the switchgear mechanism and regional changes in heat loss make the Barents Sea a key contributor to the Arctic Ocean atlantification.

Discussion

This research identifies the mechanisms driving atlantification and paints a broad and comprehensive picture of changes in the northern high-latitude climate system. Switchgear is one of these mechanisms resulting from alternating AD atmospheric regimes. We discovered increased Atlantic water inflows throughout the Barents Sea and reduced inflow across Fram Strait, which resulted in a stronger warming of the Barents Sea as compared with Fram Strait during 2007 to 2021. This regime was also associated with the amplified Beaufort Gyre, stronger boundary currents at the Siberian slope, and a shifted Transpolar Drift from the Amerasian Basin toward the Lomonosov Ridge.

One of the most notable changes associated with AD variability is the 2007 to 2021 hiatus of Arctic summer sea-ice loss, which, we argue, is a response to enhanced redistribution of freshwater into the Amerasian Basin caused by anomalous winds and increased stratification that suppress oceanic heat fluxes. This process is regionally limited to the Amerasian

Basin, where the sea-ice area has actually increased since 2007 (Fig. 1, D and E). Thus, although variations in atmospheric forcing may affect the ice-loss slowdown since 2007 (*45*), the shutting down of oceanic heat fluxes by increasing Amerasian Basin stratification (Fig. 1B, inset) may help drive the ice-loss hiatus. To validate this hypothesis, we used the winter survival of the near-surface temperature maximum created by the summer trapping of solar radiation below the surface mixed layer (10- to 30-m depth) (*46*). By using an extensive 2007 to 2020 archive of Ice-Tethered Profiler observations, we found that 65% of vertical temperature profiles showed the presence of the near-surface temperature maximum (and therefore negligible upper Amerasian Basin ventilation) during October to March (fig. S14; see materials and methods for details)—a convincing argument that enhanced sea-ice winter growth owing to reduced ocean heat fluxes contributed to the observed 2007 to 2021 ice-loss hiatus. Sea-ice dynamics should not be disregarded, however. For example, despite increased ice-area export (Fig. 2D), decreased ice thickness in the Fram Strait (*10*) may cause a decline in ice volume export, which would offset the decline in net ice production in high-latitude regions (*47*). In contrast to the Amerasian Basin, ventilation of the upper Eurasian Basin in the 2010s is well documented (*5*, *9*, *36*), and sea-ice loss in this basin continued through the 2010s (Fig. 1, D and E).

There are numerous ongoing and potential ecological consequences of the observed physical changes. For example, the summer-integrated normalized difference vegetation index (TI-NDVI), a remotely sensed proxy for Arctic vegetation productivity, shows markedly different behavior during AD+ and AD–. The TI-NDVI trends at all longitudes were primarily positive in 1992 to 2006, which suggests that the vegetation gained biomass and photosynthetic productivity increased; the vegetation was "greening" (Fig. 1, C and F). In 2007 to 2021, negative trends dominated the area between 210°E to 300°E (corresponding to the Amerasian Basin sector where sea ice increased during 2007 to 2021), which suggests that the vegetation lost biomass and was possibly less vigorous, often called "browning" (Fig. 1, D and F). Thus, sea-ice variability can influence Arctic vegetation productivity on numerous timescales, which is consistent with a correlation between the TI-NDVI and spring sea-ice variations (*48*).

Furthermore, the import of subarctic waters has profound impacts on Arctic marine life (*49*), and both the Fram Strait and the Barents Sea Opening branches are potential pathways of subarctic-boreal organisms into the eastern Eurasian Basin (*50*). Our results suggest that organisms drifting in the upper 50 m of the Fram Strait branch had a fundamentally different fate if entering during AD– as compared with AD+ (Fig. 4, D and E). During AD–, most organisms entered the western Eurasian Basin via the Transpolar Drift, whereas during AD+, they were kept at the shelf break and transported into the eastern Eurasian Basin. In addition, during AD+, more organisms entered the eastern Eurasian Basin from the Barents Sea (Fig. 4E). An increased influence of the Barents Sea may cause the eastern Eurasian Basin to be more productive and provide more suitable living conditions for subarctic-boreal species than its western part (*51*), which is consistent with recent observations (*50*). Improved knowledge of asymmetric conditions in the pelagic ecosystems of the western and eastern Eurasian Basin is imperative to properly understand and manage the central Arctic Ocean fisheries agreement established in 2021.

In addition, we note that recent atmospheric changes as indicated with a shifting AD phase have been important drivers of the regional patterns of sea-ice and oceanic responses. There are, however, indications that the Arctic system may be entering another regime (see wavelets in figs. S3, S7, and S8), with potential consequences for the state of the physical, chemical, and biological components. The transition may be abrupt, similar to the rapid changes in 2007. The trajectory of the Arctic climate system into the future is further complicated by the existence of large-amplitude, multidecadal variability (fig. S15). Thus, accurate future projections require a comprehensive understanding of complex air-ice-ocean interactions and associated feedback mechanisms on broad spatio-temporal scales through advancement of the observing system and modeling capabilities.

REFERENCES AND NOTES

1. IPCC, *Climate Change 2022: Impacts, Adaptation, and Vulnerability. Contribution of Working Group II to the Sixth Assessment Report of the Intergovernmental Panel on Climate Change*, H.-O. Pörtner, D. C. Roberts, M. Tignor, E. S. Poloczanska, K. Mintenbeck, A. Alegría, M. Craig, S. Langsdorf, S. Löschke, V. Möller, A. Okem, B. Rama, Eds. (Cambridge Univ. Press, 2022).
2. Q. Shu *et al*., *Sci. Adv.* **8**, eabn9755 (2022).
3. R. A. Woodgate, T. Weingartner, R. Lindsay, *Geophys. Res. Lett.* **37**, L01602 (2010).
4. K. Shimada *et al*., *Geophys. Res. Lett.* **33**, L08605 (2006).
5. I. V. Polyakov *et al*., *Science* **356**, 285–291 (2017).
6. I. V. Polyakov *et al*., *Front. Mar. Sci.* **7**, 491 (2020).
7. R. B. Ingvaldsen *et al*., *Nat. Rev. Earth Environ.* **2**, 874–889 (2021).
8. V. Ivanov *et al*., *J. Phys. Oceanogr.* **46**, 1437–1456 (2016).
9. I. V. Polyakov *et al*., *J. Clim.* **33**, 8107–8123 (2020).
10. H. Sumata, L. de Steur, D. V. Divine, M. A. Granskog, S. Gerland, *Nature* **615**, 443–449 (2023).
11. R. Kwok *et al*., *J. Geophys. Res.* **114**, C07005 (2009).
12. R. Kwok, *Environ. Res. Lett.* **13**, 105005 (2018).
13. S. Kacimi, R. Kwok, *Geophys. Res. Lett.* **49**, e2021GL097448 (2022).
14. B. Wu, J. Wang, J. E. Walsh, *J. Clim.* **19**, 210–225 (2006).
15. J. Zhang, R. Lindsay, M. Steele, A. Schweiger, *Geophys. Res. Lett.* **35**, L11505 (2008).
16. J. E. Overland, M. Wang, *Tellus Ser. A Dyn. Meterol. Oceanogr.* **62**, 1–9 (2010).
17. L. H. Smedsrud, M. H. Halvorsen, J. C. Stroeve, R. Zhang, K. Kloster, *Cryosphere* **11**, 65–79 (2017).
18. J. E. Overland, M. Wang, *Geophys. Res. Lett.* **32**, L23808 (2005).
19. J. E. Overland, M. Wang, S. Salo, *Tellus Ser. A Dyn. Meterol. Oceanogr.* **60**, 589–597 (2008).
20. J. Wang *et al*., *Geophys. Res. Lett.* **36**, L05706 (2009).
21. M. Tsukernik, C. Deser, M. Alexander, R. Tomas, *Clim. Dyn.* **35**, 1349–1360 (2010).
22. J. Morison *et al*., *J. Phys. Oceanogr.* **51**, 1053–1075 (2021).
23. V. S. Lien, F. B. Vikebø, O. Skagseth, *Nat. Commun.* **4**, 1488 (2013).
24. M. Muilwijk, L. H. Smedsrud, M. Ilicak, H. Drange, *J. Geophys. Res. Oceans* **123**, 8159–8179 (2018).
25. M. Muilwijk *et al*., *J. Geophys. Res. Oceans* **124**, 6286–6322 (2019).
26. S. Broomé, L. Chafik, J. Nilsson, *J. Geophys. Res. Oceans* **126**, e2021JC017248 (2021).
27. D. L. Volkov, T. V. Belonenko, V. R. Foux, *Geophys. Res. Lett.* **40**, 738–743 (2013).
28. P. K. Jakobsen, M. H. Ribergaard, D. Quadfasel, T. Schmith, C. W. Hughes, *J. Geophys. Res.* **108**, 3251 (2003).
29. L. Chafik, J. Nilsson, Ø. Skagseth, P. Lundberg, *J. Geophys. Res. Oceans* **120**, 7897–7918 (2015).
30. A. Proshutinsky *et al*., *J. Geophys. Res. Oceans* **124**, 9658–9689 (2019).
31. R. A. Woodgate, *Prog. Oceanogr.* **160**, 124–154 (2018).
32. S. B. Hall, B. Subrahmanyam, M. Steele, *J. Geophys. Res. Oceans* **128**, e2022JC019247 (2023).
33. I. V. Polyakov, M. Mayer, S. Tietsche, A. Y. Karpechko, *J. Clim.* **35**, 2849–2865 (2022).
34. J. Morison *et al*., *Nature* **481**, 66–70 (2012).
35. M. B. Alkire, J. Morison, R. Andersen, *J. Geophys. Res. Oceans* **120**, 1573–1598 (2015).
36. I. V. Polyakov *et al*., *Geophys. Res. Lett.* **47**, e2020GL089469 (2020).
37. L. H. Smedsrud *et al*., *Rev. Geophys.* **60**, e2020RG000725 (2022).
38. H. Hátún, A. B. Sandø, H. Drange, B. Hansen, H. Valdimarsson, *Science* **309**, 1841–1844 (2005).
39. N. P. Holliday *et al*., *J. Geophys. Res. Oceans* **120**, 5945–5967 (2015).
40. K. A. Orvik, *Geophys. Res. Lett.* **49**, e2021GL096427 (2022).
41. B. I. Barton, Y.-D. Lenn, C. Lique, *J. Phys. Oceanogr.* **48**, 1849–1866 (2018).
42. K. A. Mork *et al*., *Geophys. Res. Lett.* **41**, 6221–6228 (2014).
43. G. W. K. Moore, K. Våge, I. A. Renfrew, R. S. Pickart, *Nat. Commun.* **13**, 67 (2022).
44. Ø. Skagseth *et al*., *Nat. Clim. Chang.* **10**, 661–666 (2020).
45. J. A. Francis, B. Wu, *Environ. Res. Lett.* **15**, 114034 (2020).
46. J. M. Jackson, W. J. Williams, E. C. Carmack, *Geophys. Res. Lett.* **39**, L03603 (2012).
47. J. Zhang, *Geophys. Res. Lett.* **48**, e2021GL094780 (2021).
48. U. S. Bhatt *et al*., *Environ. Res. Lett.* **16**, 055019 (2021).
49. B. A. Bluhm *et al*., *Front. Mar. Sci.* **7**, 544386 (2020).
50. P. Snoeijs-Leijonmalm *et al*., *Sci. Adv.* **8**, eabj7536 (2022).
51. R. B. Ingvaldsen *et al*., *Sci. Rep.* **13**, 1000 (2023).
52. S. K. Gulev *et al*., in *Climate Change 2021 – The Physical Science Basis Working Group I Contribution to the Sixth Assessment Report of the Intergovernmental Panel on Climate Change* (Cambridge Univ. Press, 2023), pp. 287–422.
53. Q. Wang *et al*., *Ocean-Land-Atmos. Res.* **2**, 0013 (2023).

ACKNOWLEDGMENTS

Funding: This study was supported by NSF grant no. 1724523 (A.V.P. and I.V.P.) and ONR grant no. N00014-21-1-2577 (I.V.P.). J.A.F. was supported by funding from the Woodwell Climate Research Center. Support for R.B.I. was provided by the Research Council of Norway through the Nansen Legacy project (276730) and Institute of Marine Research, Norway. U.S.B. was supported by NASA's Arctic Boreal Vulnerability Experiment initiative under grant 80NSSC22K1257. Ø.S. received support from RCN grant no. 295962 NorEMSO. **Author contributions:** All authors participated in data processing and preliminary analysis; A.V.P. and I.V.P. carried out statistical analysis of reanalysis and mooring data from

the eastern Eurasian Basin, R.K. provided sea-ice analysis and processing, M.J. provided help interpreting Fram Strait data and formulating objective of the study, J.A.F. supervised processing and analysis of atmospheric data, Ø.S. and R.B.I. provided processing and analysis of data from the Nordic and Barents seas, and U.S.B. added multidisciplinary data and discussion. All authors contributed to interpreting the data and writing the paper.
Competing interests: The authors declare no competing interests.

Data and materials availability: All data used in the analysis are available as described in the supplementary materials. Correspondence and requests should be addressed to I.V.P.

SUPPLEMENTARY MATERIALS

science.org/doi/10.1126/science.adh5158
Materials and Methods
Figs. S1 to S15
References (*54*–*73*)

Submitted 9 March 2023; accepted 19 July 2023
10.1126/science.adh5158